DOI: 10.1007/s12541-012-0056-9

Selective Laser Sintering of a Hydroxyapatite-silica Scaffold on Cultured MG63 Osteoblasts in Vitro

Fwu-Hsing Liu[1], Yung-Kang Shen[2,#] and Jeou-Long Lee[3]

1 Department of Mechanical Engineering, Lunghwa University of Science and Technology, 33306, Taiwan
2 School of Dental Technology, College of Oral Medicine, Taipei Medical University, 11031, Taiwan
3 Department of Chemical and Material Engineering, Lunghwa University of Science and Technology, 33306, Taiwan
Corresponding Author / E-mail: ykshen@tmu.edu.tw, TEL: +886-2-27361661ext.5147, FAX: +886-2-27362295

KEYWORDS: Ceramics, Scanning electron microscopy (SEM), Powder processing, Sol-gel methods

This study forms hydroxyapatite-silica ceramic structure, which can generate interconnected porous 3D models suitable as bone scaffold, using a novel selective laser sintering (SLS) technique. Hydroxyapatite (HA) powder and a silica sol are first mixed into slurries. After processing by SLS, the HA particles are embedded in the gelled silica matrix to form green parts. The processed parts are analyzed by scanning electron microscopy (SEM). The number of cells attached on this scaffold surface is obtained by the in vitro cultured cells test. The higher number of viable cells are obtained when the sintering temperature of the scaffold was 1200°C at day 4 of cell culturing. The proposed technology can be applied to generate a bone scaffold model of porous bio-ceramics for biomedicine.

Manuscript received: February 14, 2011 / Accepted: September 28, 2011

1. Introduction

Metals, polymers, and ceramics are common implant materials. An obvious drawback of these materials is the difficulty attaching an implant to surrounding bone tissue. Implants are typically attached to bone with a screw, which can damage bone via stress concentrations.[1] However, bioactive materials containing an apatite phase can be attached by a more suitable method, the proposed method, to form a secure physical bond with tissue surrounding an implantation and can be tailored to have mechanical properties similar to those of human bone.[2] Additionally, bioceramics have been widely utilized as bone replacement materials due to their excellent biocompatibility. Further, bioceramics are considered appropriate scaffold materials by many researchers.[3,4]

Conventional implant fabrication processes generate a limited number of implant types for surgeons to choose and offer simpler modify implant site than the implant itself.[5] A significant problem associated with these restrictions is the degree of skeletal adaptation. Therefore, a new method that generates a customized model and produces suitable implants is highly desirable. One goal of this study is to investigate the use of rapid prototyping (RP) with bioceramic materials to build bone scaffolds that are tailored to individual patients.

Traditional processing methods model bone replacement materials; however, precise control of the internal architecture, such as pore size, pore shape, and interconnectivity, is lacking.[6] Some method for fabricating scaffolds, such as solvent casting, gas forming, and freeze-drying, can generate interconnected micro-pores, but lack both precision and reproducibility.[7,8] To overcome these shortcomings, layer manufacturing technologies are suitable for generating tissue scaffolds or bone replacement materials because complex shapes are easily constructed with these technologies. Notably, RP techniques can construct physical objects from three-dimensional (3D) Computer-Aided Design (CAD) data, allowing designers to create original prototypes rather than two-dimensional (2D) images. General advantages of RP techniques are rapid construction of a prototype with complex shapes from a concept.

Various RP technologies are used to construct parts made of polymer, metal, or ceramics without special tools or molds.[9] Therefore, the goal of this study is to investigate the feasibility of using selective laser sintering (SLS) to construct a porous bone scaffold using bioactive ceramics. Additionally, this study observes the behavior of osteoblast-like cells (MG63) cultured on a bone scaffold. Observation results show that cell adhesion and spreading are influenced by a surface topography with nanometer features.

2. Methods and Materials

2.1 Selective laser sintering

The SLS technique uses a laser beam to sinter/fuse powder particles to form a solid part. By spreading thin layers of powder-based materials and repeating the laser sintering process, a 3D model is fabricated layer by layer. Therefore, SLS is becoming a popular technique for producing metals, ceramics, composites, and their applications due to the wide availability of materials.

In this study, a CO_2 laser is utilized to sinter a ceramic slurry mixed with hydroxyapatite (HA) powder and a ceramic silica binder. When a silica binder is evaporated by a laser beam, curing occurs, and the binder then bonds HA particles to form a solid body, while the un-scanned portion remains a slurry.

A layer manufacturing process that was developed for forming a glass-ceramic HA-silica part. The process (Fig. 1) has the following steps. (a) The HA powder and silica binder are blended as raw materials in the ceramic slurry. (b) The slurry is paved by a scraper onto the elevator to form a thin slurry layer. (c) The spread slurry layer is selectively sintered via a CO_2 laser beam according to sliced 2D patterns from a 3D CAD mold. A solid ceramic layer is formed by curing. (d) The working platform of the apparatus is lowered by an elevator to the thickness of the monolayer. (e) Steps (b)-(d) are repeated, and a multi-layer part is obtained by stacking cured layers. (f) The residual slurry is removed and a green 3D bioceramic part is then obtained.[10,11]

When a process is developed for fabricating bioactive materials, process parameters must be optimized. A factor important to the success of the laser sintering process is control of laser radiation energy. Laser energy density at the layer surface is derived via the following equation:[12]

$$\text{Energy density (J/mm}^2\text{)} = {}^{P}\!/_{VS \times HS} \quad (1)$$

where P is laser power, VS is laser scanning speed, and HS is laser hatch spacing.

A range of parameters can be altered in the laser forming process as follows: laser power varied at 3-25 W; scan speed range was 20-250 mm/s; laser hatch spacing varied at 0.1-0.2 mm; and, layer thickness varied at 50-150μm.

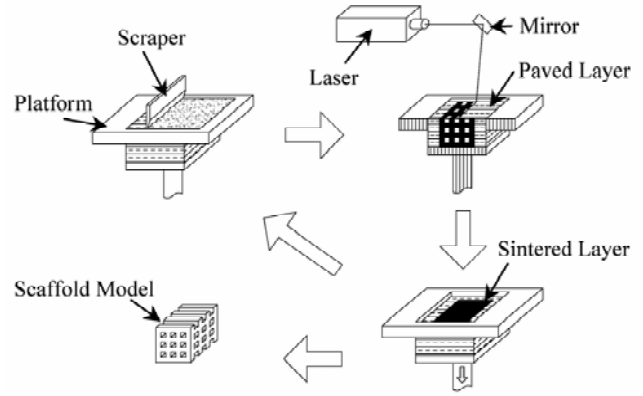

Fig. 1 Schematic of a bioceramic manufacturing processes of selective laser sintering

2.2 Experimental setup

Figure 2 shows a schematic diagram of the rapid prototyping system. The setup comprised a laser scanning system, a material spreading system, and a control system. The laser scanning system consisted of a CO_2 laser with a power output of 25 W and a laser scanner with a scan field of 125×125mm^2. The laser tube and laser scanner were controlled by a laser control card in a personal computer.[13]

2.3 Hydroxyapatite and silica slurry

The criteria for biomaterial selection focused on glass-ceramic bioactivity. The biomaterial selection was determined from an apatite phase that exists in the following three material groups: ceramic HA, glass-ceramic apatite-wollastonite (A-W), and apatite-mullite (A-M).[5] Conversely, three materials, powder, liquid, and solid-based phase, can be used with RP technology. However, another material was employed in this research. The ceramic slurry material, comprising silica sol and HA powder with average particle diameters of 5 μm, was used in the following experiments. The HA powder and silica binder were mixed in a proportion of 30-70 wt. % to obtain a compound slurry with a suitable viscosity. Table 1 shows the ratio of each component in the slurry.

The reasons for using a bioceramic slurry in the laser sintering process are twofold. First, the composition of ceramic glass is $SiO_2 \cdot P_2O_5 \cdot CaO$ has the potential to produce synthetic bone scaffold structures as a result of their sufficient biocompatibility. Second, these slurries have enhanced flexibility and viscosity during the formation processing, and are easily spread as a thin ceramic layer and to construct a green porous structure, particularly, interconnected pores.

2.4 Cell culture

Human osteogenic sarcoma (MG63, ATCC CRL-1427) was maintained in Dulbecco's modified Eagle Medium (DMEM) (HyClone, UK) with 10% heat-inactivated Fetal Bovine Serum (FBS) (Sigma, USA). Prior to confluence, osteoblasts were harvested from the monolayer culture with 0.25% trypsin EDTA (Sigma, country). Trypsin was neutralized with 10% FBS in

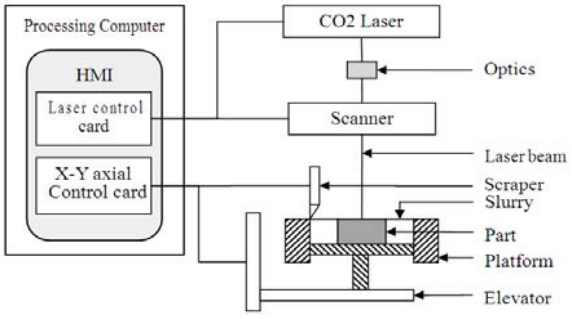

Fig. 2 Schematic of the rapid prototyping system for forming bioceramic parts

Table 1 The composition of HA-silica ceramic glass

	O	Si	P	Ca
Wt%	44.59	19.84	7.84	27.73

DMEM. Each substrate was sterilized with 70% ethanol. Osteoblasts (< 15 doublings) were seeded onto substrates at a density of 5000 cells ml-1 in DMEM supplemented with 10% FBS. After 24 h, cells were fixed using 4% paraformaldehyde. Cells were then processed for fluorescent staining of actin filaments and nuclei with TRITC-conjugated Phalloidin and DAPI using a staining kit (FAK100; Chemicon International, USA) according to the manufacturer's protocol. Substrates were then washed with buffer to remove loosely bound cells prior to imaging. This study observed morphological results of cell culturing for 4 h, 1 d and 4 d by scanning electron microscopy (SEM) (JSM-6700F; JOEL, Japan). This study also applied the microculture tetrazolium test (MTT) assay to assess cell activity. The MTT assay measures optical density (OD). The OD value indicates the activity of particle glanda; that is, the number of live cells. This study used an ELISA reader (Anthos 2020) to determine the OD value at 4 h, 1 d, and 4 d.

3. Results and Discussions

3.1 Laser curing effect

To achieve cure the silica binder, mixed HA-silica ceramic slurries were dried at room temperature, forming a solid after 12 h. The specimen was then placed in a furnace at 150°C for 2 h to remove moisture. Figure 3 shows the fractured specimen surface, confirming that curing the silica binder can bond HA particles together to form a solid body. Although many cavities are distributed in this structure, it has no layer boundary.

During the laser sintering process, curing occurs when the surface of bioceramic slurries receive sufficient laser energy to cause them cure under various process parameters. While the laser beam spot was kept 0.3 mm and the layer thickness was kept constant at 0.1 mm, the margin of overlapping between subsequent cured lines, laser scanning speed, and laser output energy were all defined the range. To construct a single layer, the laser scans serous of overlap lines were cured together to form an HA-silica mono layer. The line overlap varied at 75%, 50%, and 25% of beam spot width.

After the sintering processes (Fig. 1), the mixed bioceramic slurries were applied onto the platform surface and were then scraped to form a monolayer with a consistent thickness. The spread slurry layer was scanned by the laser beam. The HA powder bonded together via the cured silica binder to form a solid layer based on the slice pattern of a 3D mold.

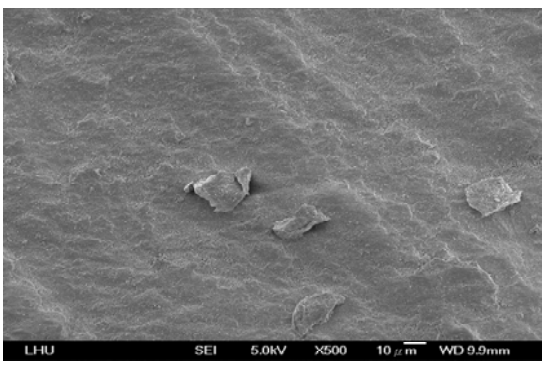

Fig. 3 SEM image showing fracture surface morphologies of the bioactive-ceramic specimen

Conversely, the un-scanned area was still in the slurry state because the silica binder was not cured. After uncure, the remaining slurry was removed from the part, and a number of cured bioceramic specimens 25mm×25mm were generated across a range of laser scan speeds; layer thickness was 100μm at a laser power of 15 W. Figure 4 show the relationship between depth of cured layers and laser scan speed.

As scan speed increased from 40 to 160 mm/s, cure depth decreased from 139 to 106μm. Table 2 lists the over-cured ratio of sintered layers obtained from experimental results under various laser scan speeds. The over-cured ratio increased as laser scan speed decreased. Additionally, an appropriate multi-layer specimen can be fabricated at low scan speeds after coherent layers were stacked. Figure 5 shows a cured specimen.

3.2 Influence of process parameters

Experimental results indicate that laser energy, laser scan speed, and scan line overlap were statistically significant. The most significant factor for flexural strength was laser energy, which positively influenced strength as laser power increased. The second most significant factor was the combination of laser energy, scan speed, and scan line overlap, which yielded laser energy density in the scanning zone.

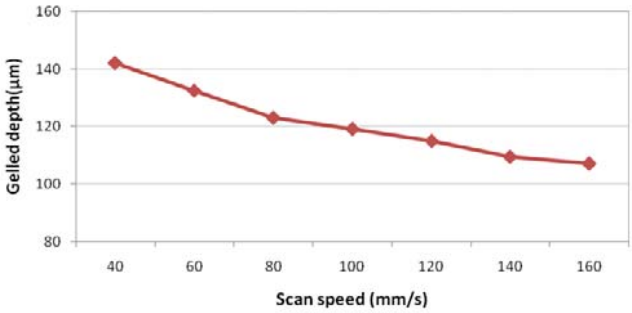

Fig. 4 The relation between cured depth and laser scan speed

Table 2 The over-cured ratio of sintered layer

Scan speed (mm/s)	40	60	80	100	120	140	160
Cured-depth (μm)	142	131	124	119	115	110	106
Layer thickness (μm)	100	100	100	100	100	100	100
Over-cured ratio (%)	42	31	24	19	15	10	6

Fig. 5 A multi-layer specimen produced by bioceramic

At a certain laser scan speed, the constructed layers were poorly cured at low laser power of 5 W. Furthermore, when laser power increased, fragility of the cured layer decreased and structural strength improved when laser energy density was sufficient.

At a fixed laser power, the shape integrity of the fabricated multi-layers increased as scan speed decreased. This improved cured bioceramic solidification at slow scan speeds and high laser power because increased energy added to the slurry surface increased curing. Thus, as scan speed increased, the amount of energy absorbed decreased. Figure 6 lists the effect of laser power relative to laser scan speed.

Further post-process tests at 1200°C for 60 min indicate that laser energy density had a significant effect on bending strength (Fig. 7), suggesting that a maximum strength of 5.6 MPa was obtained at 0.64 J/mm^2. Above 0.64 J/mm^2, laser energy was too great, degrading silica gelled and reducing strength. At 0.64-0.5 J/mm^2, energy density was sufficient to gel the silica sol; therefore, bending strength increased as laser density increased. At < 0.5 J/mm^2, the slurry layer did not form due to insufficient energy density, resulting in partial gelling of the silica sol.

3.3 Fabrication porous scaffolds

Experimental results indicate that a feasible parameter window is as follows: laser power of 8-16 W; laser scan speed of 95-160 mm/s; and, scan hatch spacing of 0.15-0.2 mm. The process parameters that generated 100-μm-thick layers were laser power of 16W, scan speed of 125 mm/s, and hatch spacing of 0.15 mm, confirming the ability of the laser curing process to produce green HA-silica glass parts with an interconnected pore structure (Fig. 8).

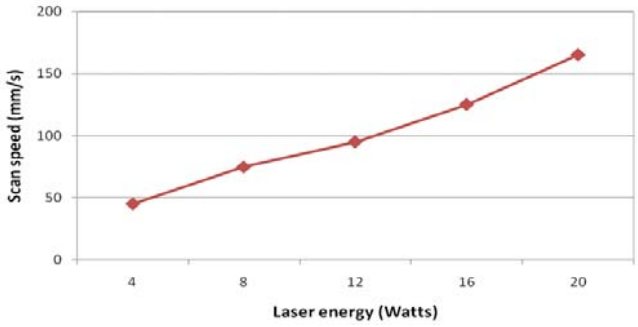

Fig. 6 Block diagram of multi-modal chatter model of a high speed machining center

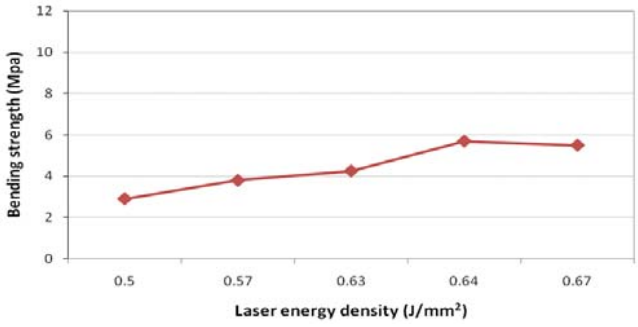

Fig. 7 Main effects plot for bending strength with regard to laser energy density

These parts had a surface finish of 25μm and a dimensional variation at 15%. Total fabrication time was 120 min; notably, this part can be built relatively faster by SLS.

The as-manufactured HA-silica parts confirm that the porous structure can be achieved and, thus, the potential for bone ingrowth is promising. The interconnected pores with diameters of 1-2 mm can be generated to support vascularization. The mechanical strength of implants is adversely affected by high porosity. Therefore, a balance between pore size and strength of the scaffold model is required for implant applications.

The primary aim of this study is to demonstrate the feasibility of the laser curing process for fabricating HA-silica glass ceramic scaffold with a porous structure and generate parts for use as bone scaffolds. The major requirement is the ability to generate an interconnected porous structure with pores in the range of 100-600μm to support bone growth.[14,15] The SEM micrograph of the bioceramic samples indicates that the structure was achieved (Fig. 9). A number of pores of various shapes formed in the ceramic matrix. Figure 9 shows SEM micrographs of the bio-glass surface.

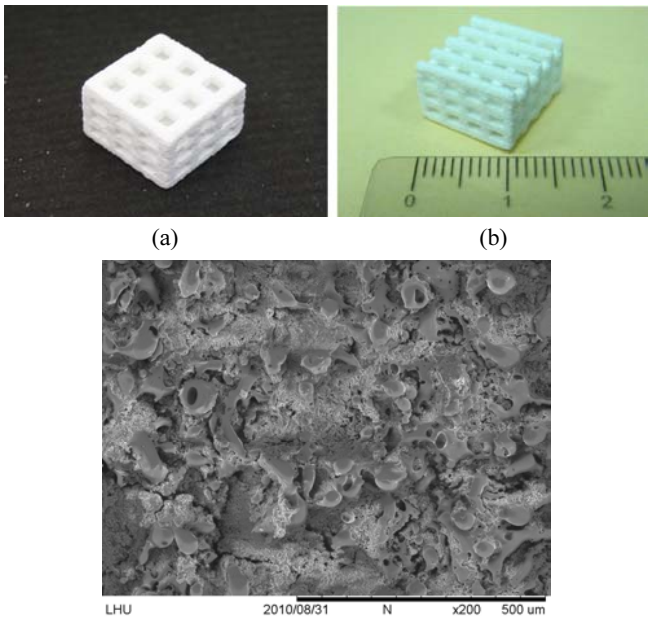

(a) (b)

(c)

Fig. 8 The HA-Silica scaffold models with interconnective porous obtained by SLS: (a) and (b) an actual part; (c) an SEM image of the pores structure inside the surface of laser-sintered bone scaffolds

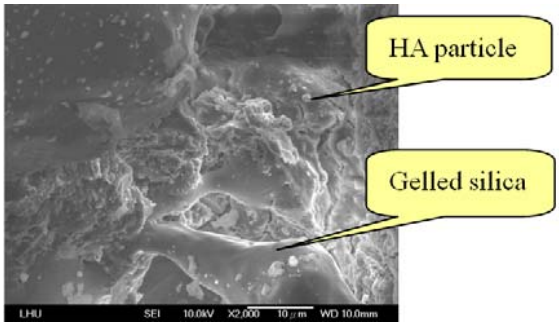

Fig. 9 SEM micrograph of the surface of a bio-glass part generated by HA particles and gelled silica

The HA particles were embedded in the ceramic-matrix of gelled silica.

Notably, micro-porosity can also be generated using the laser curing technique. However, high porosity can negatively affect the strength of delicate bone scaffolds; thus, one must achieve a balance between porosity for bone ingrowth and mechanical strength to avoid scaffold failure.

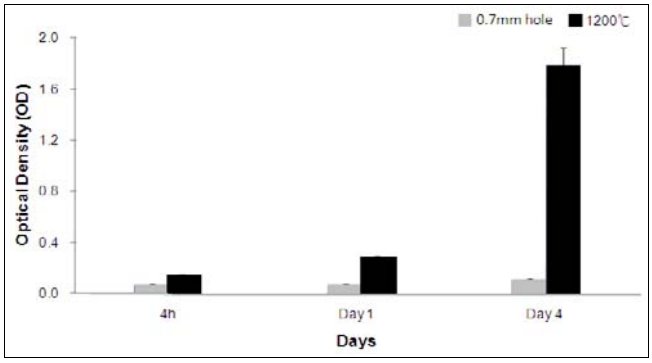

Fig. 10 MTT assay for osteoblast-like cell

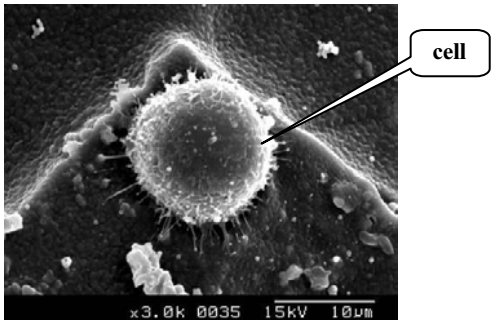

(a) 4hours

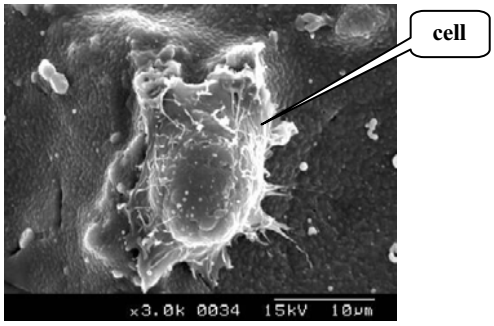

(b) Day 1

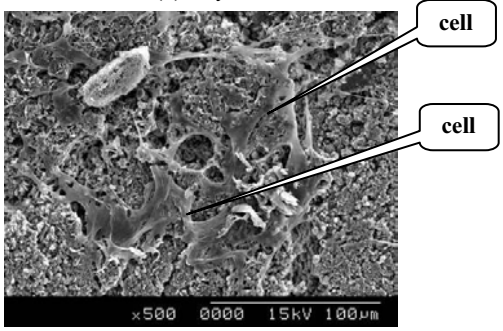

(c) Day 4

Fig. 11 SEM image for cell behavior on the surface of bioceramic scaffold after sintering at 1200°C: (a) cell adhesion at 4 hours, (b) spreading at day 1, and (c) filopodia elongation at day 4

3.4 Cell culture

Cells were cultured on the green part and sintered bone scaffolds after heat treatment at 1200°C to achieve maximum flexural strength. Figure 10 shows cell culturing results by MTT assay. The OD values of the sintered scaffold were larger than that of the green part, indicating that a sintered scaffold can contribute more to cell growth.

To investigate the effect of topography on cell-scaffold interaction, human osteogenic sarcoma cells were cultured on sintered bone scaffolds and their morphology was analyzed. The behaviors of cell growths were adhesion at 4 h, spreading at d 1, and filopodia elongation at d 4 (Fig. 11).

4. Conclusions

A comparison of RP technologies for production of HA-silica ceramic parts indicates that the forming process has three features. First, bio-ceramic samples can be fabricated rapidly via a layer manufacturing process. The proposed process differs from traditional methods for generating bio-ceramic materials. Second, the laser curing process uses slurries as raw materials to fabricate scaffolds. Therefore, the slurry possesses flexibility that is easily formed in interconnected porous bone scaffolds to support bone cell growth. Experimental results can be rationalized in terms of the ability of cells to form effective adhesion complexes on the surface of a porous scaffold after heat treatment at 1200°C. This study demonstrates that the RP scaffold is a feasible method to construct surfaces that resist cell spreading and adhesion, which can be useful for cell culturing, bio-MEMs, and implant devices that involve biological and abiological interfaces.

ACKNOWLEDGEMENT

This work was supported by the National Science Council of the Republic of China, Taiwan, under Contract Nos. NSC 99-2221-E-262-003 and NSC 98-2221-E-038-001. We also gratefully acknowledge financial support from the Ministry of Education of the Republic of China, Taiwan, under Contract No. 99M-88-067.

REFERENCES

1. Xiao, K., Dalgarno, K. W., Wood, D. J., Goodridge, R. D. and Ohtsuki, C., "Indirect selective laser sintering of apatite-wollost onite glass-ceramic," Proceedings of the Institution of Mechanical Engineers Part H: Journal of engineering in medicine, Vol. 222, No. 7, pp. 1107-1114, 2008.
2. Babini, G. N., Bellosi, A. and Vincenzini, P., "Oxidation of silicon nitride hot pressed with Y_2O_3+MgO," J. Mater. Sci., Vol. 18, No. 1, pp. 231-244, 1983.
3. Cyster, L. A., Grant, D. M., Howdle, S. M., Rose, F. R. A. J., Irvine, D. J., Freeman, D. and Shakesheff, K. M., "The

influence of dispersant concentration on the pore morphology of hydroxyapatite ceramics for bone tissue engineering," Biomaterials, Vol. 26, No. 7, pp. 697-702, 2005.

4. Almirall, A., Larrecq, G., Delgado, J. A., Martínez, S., Planell, J. A. and Ginebra, M. P., "Fabrication of low temperature macroporous hydroxyapatite scaffolds by foaming and hydrolysis of an α-TCP paste," Biomaterials, Vol. 25, No. 17, pp. 3671-3680, 2004.
5. Lorrison, J. C., Dalgarno, K. W. and Wood, D. J., "Processing of an apatite-mullite glass-ceramic and an hydroxyapatite/ phosphate glass composite by selective laser sintering," J. Mater. Sci. Mater. Med., Vol. 16, No. 8, pp. 775-781, 2005.
6. Yang, S. F., Leong, K. F., Du, Z. H. and Chua, C. K., "The design of scaffolds for use in tissue engineering. Part I. Traditional factors," Tissue Eng., Vol. 7, No. 6, pp. 679-689, 2001.
7. Ho, M. H., Kuo, P. Y., Hsieh, H. J., Hsien, T. Y., Hou, L. T., Lai, J. Y. and Wang, D. M., "Preparation of porous scaffolds by using freeze-extraction and freeze-gelation methods," Biomaterials, Vol. 25, No. 1, pp. 129-138, 2004.
8. Chen, V. J. and Ma, P. X., "Nano-fibrous poly (L-lactic acid) scaffolds with interconnected spherical macropores," Biomaterials, Vol. 25, No. 11, pp. 2065-2073, 2004.
9. Chua, C. K. and Leong, K. F., "Rapid Prototyping: Principles and Applications in Manufacturing," John Wiley & Sons, 1997.
10. Liu, F. H. and Liao, Y. S., "Fabrication of inner complex ceramic parts by selective laser gelling," J. Eur. Ceram. Soc., Vol. 30, No. 16, pp. 3283-3289, 2010.
11. Liu, F. H., "Manufacturing porous multi-channel ceramics by laser gelling," Ceram. Int., Vol. 37, No. 7, pp. 2789-2794, 2011.
12. Williams, J., Miller, D. and Deckard, C., "Selective laser sintering part strength as a function of Andrew number, scan rate and spot size," Proc. of the Solid Freeform Fabrication Symposium, pp. 549-557, 1996.
13. Liu, F. H., Shen, Y. K. and Liao, Y. S., "Selective laser gelation of ceramic–matrix composites," Compos. Part B: Engineering, Vol. 42, No. 1, pp. 57-61, 2011.
14. Gauthier, M. J., Bouler, E., Arguado, E., Pilet, P. and Daculsi, G., "Macroporous biphasic calcium phosphate ceramic: influence of macropore diameter and macroporosity percentage on bone ingrowth," Biomaterials, Vol. 19, No. 1-3, pp. 133-139, 1998.
15. Park, S., Kim, G. H., Jeon, Y. C., Koh, Y. H. and Kim, W. D., "3D polycaprolactone scaffolds with controlled pore structure using a rapid prototyping system," J. Mater. Sci. Mater. Med., Vol. 20, No. 1, pp. 229-234, 2009.